aerospace

MDPI

Article

Investigation of Spray Characteristics for Detonability: A Study on Liquid Fuel Injector and Nozzle Design

Myeung Hwan Choi [1], Yoojin Oh [2] and Sungwoo Park [2,*]

[1] BK21 FOUR Smart Drone Convergence, Korea Aerospace University, Goyang 10540, Republic of Korea; nuclearreaction@hanmail.net
[2] Department of Smart Air Mobility, Korea Aerospace University, Goyang 10540, Republic of Korea; wlsdb34@naver.com
* Correspondence: sungwoo.park@kau.ac.kr

Abstract: Detonation engines are gaining prominence as next-generation propulsion systems that can significantly enhance the efficiency of existing engines. This study focuses on developing an injector utilizing liquid fuel and a gas oxidizer for application in detonation engines. In order to better understand the spray characteristics suitable for the pulse detonation engine (PDE) system, an injector was fabricated by varying the Venturi nozzle exit diameter ratio and the geometric features of the fuel injection hole. Analysis of high-speed camera images revealed that the Venturi nozzle exit diameter ratio plays a crucial role in determining the characteristics of air-assist or air-blast atomization. Under the conditions of an exit diameter ratio of R_e/R_i = 1.0, the formation of a liquid film at the exit was observed, and it was identified that the film's length is influenced by the geometric characteristics of the fuel injection hole. The effect of the fuel injection hole and Venturi nozzle exit diameter ratio on SMD was analyzed by using droplet diameter measurement. The derived empirical correlation indicates that the atomization mechanism varies depending on the Venturi nozzle exit diameter ratio, and it also affects the distribution of SMD. The characteristics of the proposed injector, its influence on SMD, and its velocity, provide essential groundwork and data for the design of detonation engines employing liquid fuel.

Keywords: atomization; liquid fuel; Sauter mean diameter; detonation; spray

Citation: Choi, M.H.; Oh, Y.; Park, S. Investigation of Spray Characteristics for Detonability: A Study on Liquid Fuel Injector and Nozzle Design. *Aerospace* **2024**, *11*, 421. https://doi.org/10.3390/aerospace11060421

Academic Editor: Tiegang Fang

Received: 15 January 2024
Revised: 1 May 2024
Accepted: 3 May 2024
Published: 23 May 2024

1. Introduction

1.1. Detonation Engine

Detonation is a phenomenon characterized by the simultaneous occurrence of shock waves and combustion in high-temperature and high-pressure environments, representing an exceptionally rapid combustion process. The unique characteristics of detonation have paved the way for the emergence of novel propulsion system concepts. Pulse detonation engines (PDEs) generate thrust using repetitive detonations, offering a structurally simplified and weight-efficient alternative to propulsion systems that require compressors and turbines. The simplicity and reduced mass of PDEs have sparked extensive research across various domains, capitalizing on these distinctive features [1–3].

For a PDE to function effectively as a propulsion system, a high frequency of detonations needs to occur within a shorter timeframe. Because of these characteristics, research has been conducted on the characteristics of the fuel injected into the engine and the fuel mixing to operate at an even higher frequency. A PDE utilizing a rotary valve for rapid actuation has been studied [4–6]. Furthermore, a valveless detonation system has been devised for PDE operation, eliminating the need for opening and closing valves [7,8]. Without the need for valve actuation, while being continuously supplied, this process requires that both the fuel and the oxidizer undergo combustion and quenching within a single cycle.

When using gaseous fuel, achieving rapid combustion within a short timeframe is relatively straightforward. However, when using liquid fuel, it is challenging to achieve a

rapid reaction with the oxidizer within a short timeframe due to the relatively extended combustion duration inherent in the characteristics of liquid fuel compared to gaseous fuel. Schauer et al. conducted hydrogen/air simulation experiments to design a PDE using kerosene-based fuels, indicating that the design of liquid fuel PDEs requires different considerations in many aspects compared to gas fuel PDEs [2].

1.2. Liquid Fuel/Oxidizer for Detonation

If the liquid fuel within the duct remains unburned within a single cycle, the unburned fuel maintains high temperatures in localized areas. This can lead to prematurely igniting incoming fuel into the duct faster than the designed ignition timing, causing combustion instability. This phenomenon closely resembles the knocking phenomenon observed in reciprocating engines that utilize gasoline. Therefore, various approaches, including the promotion of flash boiling and fuel vaporization, have been devised. Tucker et al. conducted a study on the knocking and flash vaporization of octane within a PDE [9]. When injecting liquid fuel into the duct, achieving rapid fuel vaporization and quick reactivity becomes important, making the operational characteristics of the injector as vital as in other propulsion systems. Brophy et al. conducted fundamental liquid detonation experiments using JP-10, demonstrating the need for small droplet sizes and mixing ratios [10,11]. Frolov et al. investigated the degree of detonability based on the octane rating of the fuel [12]. Fan et al. conducted research on liquid fuel PDEs using liquid fuel and gas oxidizers, studying the performance based on the geometric shape of the PDE [13]. In addition, Lu et al. indicated the importance of breakup for sustaining fuel detonability and proposed the addition of additives as a potential solution [14]. Therefore, an appropriate flow rate is essential in maintaining stable combustion over a short duration. Additionally, small droplet diameters become significant for enhanced reactivity and vaporization. Consequently, when using liquid fuel, there are many considerations for internal detonability within the PDE compared to using gaseous fuel. In addition, for rotating detonation engines (RDEs), which operate at higher frequencies to overcome the drawback of the low-frequency operating characteristics of PDEs, there is also a consideration for the use of liquid oxidizers, such as liquid oxygen, due to cooling issues. Nicholls et al. mentioned the feasibility of RDE [15], while Bykovskii et al. and Lu et al. established the concept of RDEs through continuous spin detonations [16,17]. Xue et al., Nair et al., and Kubicki et al. conducted experiments applying hypergolic propellants to RDE systems [18–20], while Heister et al. and Kindraki et al. studied the use of liquid propellants in RDEs [21,22]. Lim et al. conducted research on wall cooling in the application of RDE systems [23].

In such instances, the characteristics of injectors that spray both gas–liquid oxidizers and fuels into the combustion chamber become critical. Injectors that simultaneously use gases and liquids in propulsion systems are referred to as air-blast or air-assist injectors, and the features of these injectors are presently applied in commercialized engines. These injectors describe spray performance based on dimensionless numbers such as Weber and Reynolds numbers, as well as momentum [24–27]. Therefore, when designing PDEs operating at high frequencies and utilizing a two-phase state of fuel and oxidizer, it is essential to consider various spray characteristics.

In this study, the spray characteristics were investigated to develop an injector suitable for the valveless PDE system of liquid fuel and gaseous oxidizer. By varying key design parameters of the injector, the crucial variables affecting combustion, such as spray pattern and droplet diameter, were measured.

2. Experimental Setup

As the volume of the detonation chamber remains constant, a shorter combustion cycle requires a more rapid filling of the chamber with fuel and oxidizer. Therefore, a higher pressure of the oxidizer can be advantageous, especially at higher operating frequencies. Additionally, to rapidly charge the chamber's internal volume with oxidizer and fuel, high pressure and fast flow rates are necessary. However, high pressure and fast flow rates

impact the atomization of liquid fuel. For effective detonation, liquid fuel must be uniformly mixed with the oxidizer and fragmented into the smallest possible volume. The increased flow rates and pressure also raise the overall flow rate of oxidizer and fuel, affecting the equivalence ratio of the oxidizer and fuel mixture; this is important for initiating detonation. Thus, optimizing the chamber's filling, mixing, and flow rates is essential for obtaining a rapid detonation cycle. Consequently, experimental conditions were set based on the mentioned considerations.

The experimental conditions are presented in Table 1. Water was used as simulant for atomization, while nitrogen was employed to simulate the oxidizer. Water was pressurized to 2.0 MPa using nitrogen and then sprayed for atomization. The mass flow was regulated using a mass flow controller, providing flow rates of 2, 4, 6, and 8 g/s. For the simulated oxidizer, the flow was controlled using pressure, ranging from the minimum pressurization of 0.8 MPa to 2.0 MPa. This was performed to demonstrate injector performance under identical pressurization conditions. The chamber's pressure was maintained at room temperature and atmospheric pressure.

Table 1. Test parameter values.

Parameter	Oxidizer	Fuel
Simulant	Nitrogen	Water
ρ (kg/m^3)	1.15~14.8	1006
μ (kg/m·s)	1.78×10^{-5}	8.9×10^{-4}
σ (N/m)	-	7.28×10^{-2}
Supply pressure (MPa)	0.8–2.0	2.0
Spray pressure condition	Ambient pressure	
T (K)	298	

Figure 1 illustrates the shape of the injector used in the experiments. Fundamentally, the fuel is injected from the central column inside the injector and is first atomized by the transverse flow of the oxidizer before being sprayed into the atmosphere through a Venturi nozzle. This injector is based on research by Yan et al., who investigated detonation characteristics based on injector geometry [8]. Therefore, following the injection method outlined in that study, various variations were created to explore the spray characteristics based on the shapes of the injector and the nozzle.

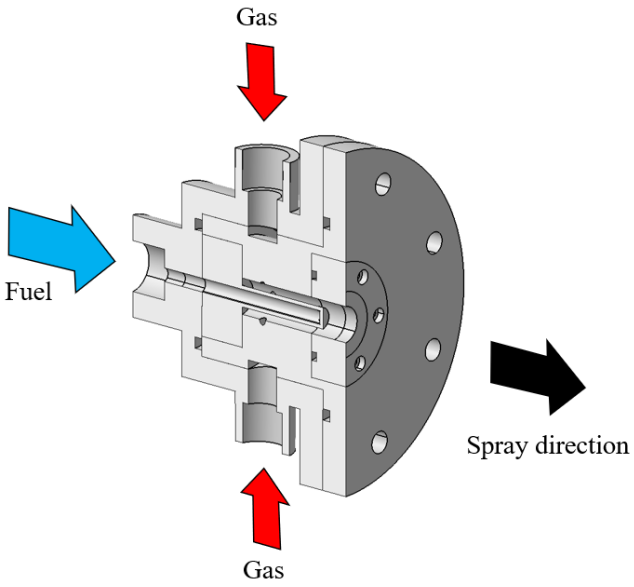

Figure 1. Schematic illustration of the overall shape of the injector ($R_e/R_i = 1.0$, Type B).

The first variation focuses on the internal fuel injection of the injector, introducing variations in the positioning of the fuel injection hole and the spraying angle. The position of the fuel injection hole was adjusted with reference to the end of the column, where the fuel is sprayed, and the angle of the spraying jet was modified. Figure 2 depicts the central columns of the four experimented injectors. In Figure 2, fuel column A has the fuel injection holes positioned at an angle of approximately 45 degrees. For type B, the fuel injection holes are located 2 mm away from the end, with a spraying angle of 90 degrees, at a perpendicular direction to the oxidizer flow. Type C is similar to type B, but the fuel injection holes are positioned 10 mm away from the end. All three types, A–C, have 4 fuel injection holes. Lastly, type D has twice as many fuel injection holes, amounting to 8 holes, and they are positioned 2 mm away from the end. The shapes of the four fuel columns are responsible for internal fuel injection within the injector, aiming to understand the resulting spray characteristics. The fuel hole diameter, represented as d_0, is consistently set to 0.5 mm for all types.

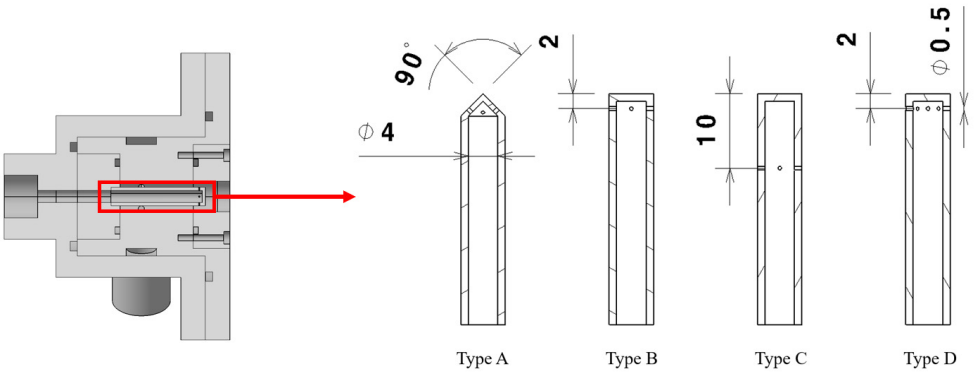

Figure 2. Four types of internal fuel injection holes (columns) configurations used in the experiment.

The second variable is the Venturi nozzle that constitutes the exit of the injector. Figure 3 illustrates the shapes of the Venturi nozzles. As shown in Figure 3, two Venturi nozzles were experimented with in this study: Figure 3a,b represent two Venturi nozzles with exit diameters of 3 mm and 10 mm, respectively. The Venturi nozzles exhibit a shape that can either contract or expand, and this was nondimensionalized. The exit diameter of the Venturi nozzle, R_e, was divided by the internal conduit diameter, R_i (which is fixed at 10 mm), and expressed as follows: Figure 3a $R_e/R_i = 0.3$; Figure 3b $R_e/R_i = 1.0$. In cases where the Venturi nozzle exit area expanded (with a diameter ratio greater than 1.0), the spray pattern became impractical for capturing images and measurements, leading to its exclusion from the experiments. Due to the nature of the injector, which utilizes air and gas to atomize fuel, the Venturi nozzle's exit area, relative to the internal flow path area of the injector, significantly affects spray characteristics. As mentioned earlier, experiments were conducted to investigate the shape variables. All the fuel columns and Venturi nozzles experimented with in this study were modulated to be applicable for subsequent multi-detonation combustion.

Figure 4 illustrates the experimental setup along with the image acquisition and average droplet diameter measurement system. The oxidizer was supplied by using a reservoir, while the fuel was delivered by using a mass flow controller. The Coriolis flowmeter (mini-CORI-FLOW M15, Bronkhorst, Achterhoek, The Netherlands), with an error margin of around 0.1%, was used for flow measurement. The injector was horizontally positioned. A Phantom Veo 710 high-speed camera from Vision Research (Vision Research, Wayne, NJ, USA) was used for spray image capture. The exposure time was set to 2.0 µs, capturing 12,000 frames per second. The captured instantaneous images were employed for the analysis of spray characteristics based on variations. Analyzing the spray images, especially using instant density gradient images showing momentary changes, provided insights into the behavior of the injector.

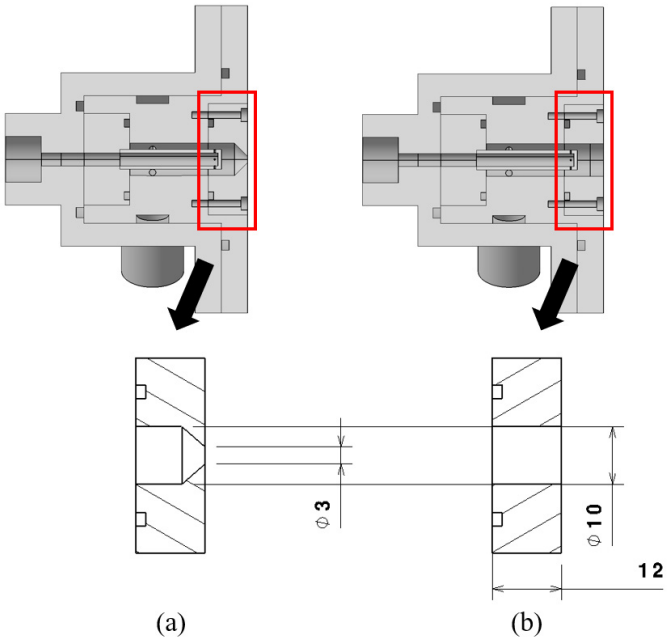

Figure 3. Geometry of the nozzle used in the experiment: (**a**) $R_e/R_i = 0.3$; (**b**) $R_e/R_i = 1.0$.

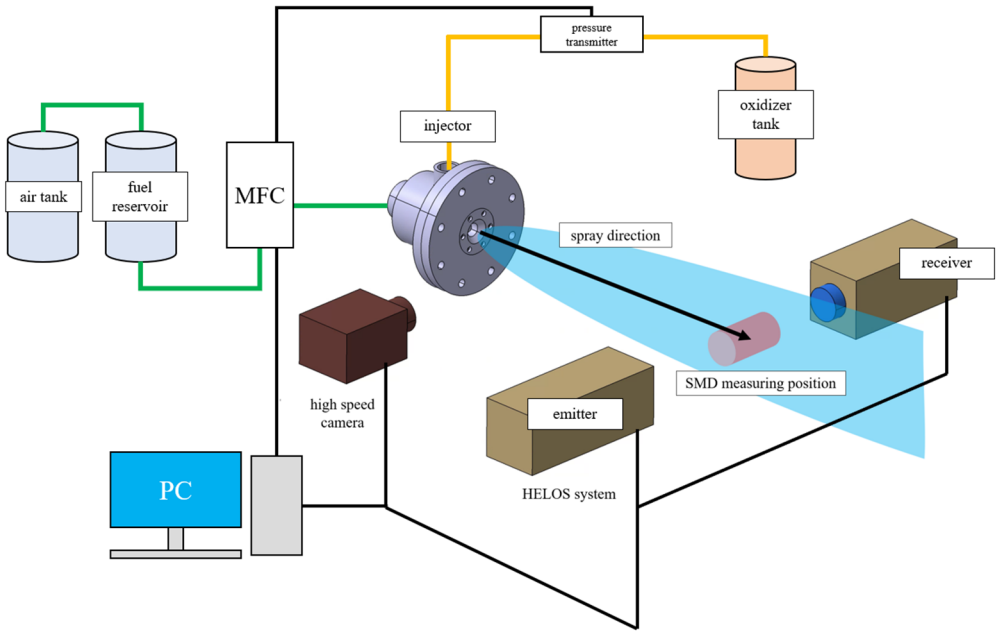

Figure 4. Schematic diagram of the experimental setup.

To determine the average droplet size, the HELOS laser diffraction system from Sympatec (Clausthal-Zellerfeld, Germany) was utilized. The measured distribution of the average droplet size follows the Rosin–Rammler distribution, allowing the calculation of Sauter mean diameter (SMD). Typically, a higher SMD increases the reaction time, while a relatively lower SMD reduces the time for reaction, providing advantages for fuel mixing. Therefore, the average droplet size, based on the injector's shape conditions and supply pressure, was expressed in terms of SMD. The measurement of the sprayed droplet size was taken at a location 50 mm away from the injector exit, mirroring the ignition position for subsequent detonation reaction experiments.

3. Results

3.1. Comparison of Venturi Nozzle Characteristics

Instead of illustrating all spray images for various injector shapes and supply rates, only a subset is presented. Figure 5 represents a case with an oxidizer supply pressure of 2.0 MPa, a fuel supply pressure of 8 g/s, and a fixed Type B fuel column. Figure 5a corresponds to the Venturi nozzle of $R_e/R_i = 0.3$, while Figure 5b corresponds to the $R_e/R_i = 1.0$. When comparing the two images, for the case with a diameter ratio of 0.3, the spray angle is narrower compared to the case with a ratio of 1.0. In the 0.3 ratio case, the density of the sprayed droplets is higher due to the narrow exit area. In the 1.0 ratio case, a relatively larger spray angle is observed, and a liquid film is formed near the exit of the Venturi nozzle. These spray characteristics indicate that fuel accumulates on the walls of the Venturi nozzle, forming a liquid film. This type of liquid film has a specific length, commonly referred to as the breakup length. The breakup length indicates the point at which a liquid jet or film undergoes disintegration, forming droplets. In this study, it is denoted as the film length. The internal fuel column of the injector used in this study is very similar to the jet in crossflow method, spraying fuel into the transverse flow field. However, if the exit area of the Venturi nozzle decreases, then it exhibits characteristics similar to an air-assist injector. These features are significantly influenced by the pressure drop at the column exit of the injector, which is determined by the upper pressure of fuel and oxidizer, impacting spray characteristics such as droplet diameter and mixer velocity.

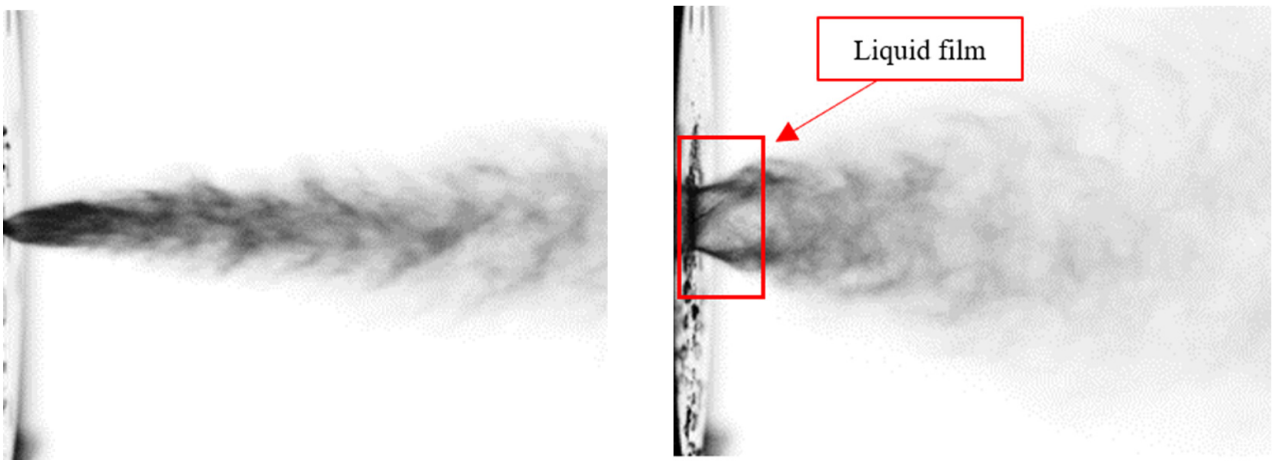

Figure 5. Instant images according to Venturi nozzle shapes: (**a**) $R_e/R_i = 0.3$; (**b**) $R_e/R_i = 1.0$.

3.1.1. Venturi Nozzle with $R_e/R_i = 0.3$

To investigate the spray characteristics based on the position of the fuel injection holes at the same angle of the Venturi nozzle, instant density gradient images are displayed in Figure 6. The conditions of the captured images represent the maximum fuel flow condition of 8 g/s and the maximum supply pressure of oxidizer at 2.0 MPa. The order of type A, B, C, and D injectors is listed in Figure 6a–d. The results of the density gradient images show that the spray characteristics do not vary significantly based on the geometric shape of the internal fuel injection holes. In the case of $R_e/R_i = 0.3$, the spray pattern is highly dependent on the exit area (ratio) of the Venturi nozzle, as explained earlier, rather than the position and shape of the internal injector flow path.

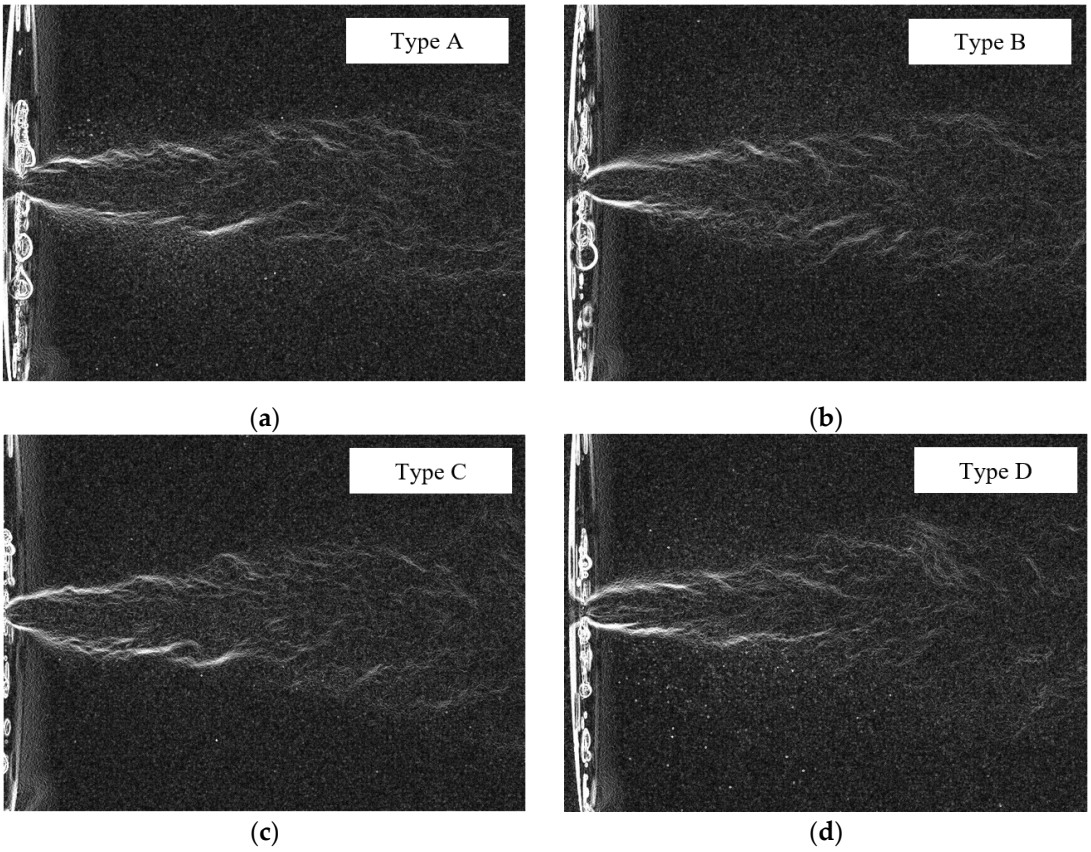

Figure 6. Density gradient images of Venturi nozzle $R_e/R_i = 0.3$, 8 g/s, 2.0 MPa: (**a**) type A; (**b**) type B; (**c**) type C; (**d**) type D.

3.1.2. Venturi Nozzle with $R_e/R_i = 1.0$

Figure 7 illustrates images captured under the conditions of maximum fuel flow rate, 8 g/s, and maximum oxidizer supply pressure, 2.0 MPa, with the Venturi nozzle diameter ratio set to $R_e/R_i = 1.0$. Two distinctive features are commonly observed in all fuel hole types: the rapid formation of a liquid film over a short distance from the Venturi nozzle and the generation of small droplets in the vicinity of the liquid film, along with their size distribution. The liquid film formed from the Venturi nozzle disintegrated into small droplets as the distance from the nozzle increases, ultimately forming a droplet cloud. The location and number of fuel injection holes influence these two characteristics.

In the case of type A, the liquid film near the nozzle is the most clearly observed compared to all other cases. Also, the number of small droplets generated from the breakup of the liquid film is the least compared to all other cases. In the case of type B, the liquid film near the Venturi nozzle is formed at a wide angle, and droplets are generated both around it and outward. In the case of type C, the liquid film formed at the Venturi nozzle exit is the shortest, and the size and quantity of droplets are the highest, with their distribution clearly observed. For type D, although it shows a spray pattern very similar to type B, the density of the droplets from the liquid film is slightly reduced. The difference between these two types can be explained based on the liquid flow velocity at the fuel injection hole due to the difference in the number of fuel injection holes.

In the case of the Venturi nozzle with $R_e/R_i = 1.0$, the length and size of the formed liquid film near the nozzle exit, due to the accumulation of fuel droplets, can influence the combustion initiation and detonation transition. Given the characteristics of the valveless system, where fuel and oxidizer are continuously supplied, if ignition occurs and the flame becomes fixed near the Venturi, combustion may not occur according to the intended operating cycle, leading to the formation of a continuous flame, similar to an

industrial burner. Therefore, the spray characteristics observed in the Venturi nozzle with $R_e/R_i = 1.0$ diameter can impact the occurrence of detonation.

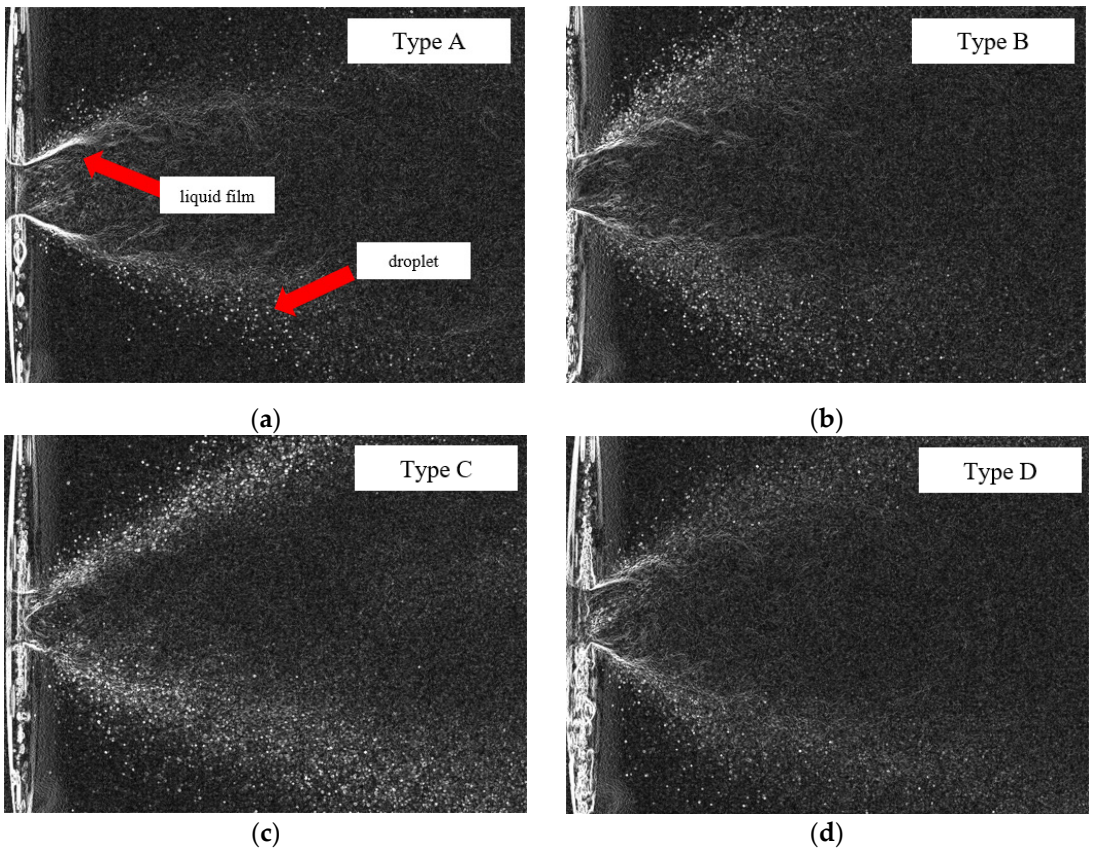

Figure 7. Density gradient images of Venturi nozzle $R_e/R_i = 1.0$, 8 g/s, 2.0 MPa: (**a**) type A; (**b**) type B; (**c**) type C; (**d**) type D.

To quantitatively evaluate the length of the liquid film, density gradient images were analyzed using Otsu's method. Figure 8 illustrates an example of this technique. Each atomization image was subjected to Otsu's technique to derive optimal threshold values and subsequently extract the threshold image. The average liquid film length was then determined from the maximum and minimum breakup lengths of this image.

Figure 9 shows the length of the liquid film formed in the Venturi nozzle with $R_e/R_i = 1.0$ in relation to the position of internal injector holes and injection pressure, depicted as Figure 9a–d for type A, B, C, and D, respectively. Generally, as the pressure increases, the length of the liquid sheet also increases. The rapid flow of oxidizer near the Venturi nozzle at this diameter ratio implies an increase in the formation of the liquid film. In the case of type C, it generally exhibits the shortest liquid film, which indicates that the influence of the position of internal fuel injector holes on the spray varies depending on the nozzle diameter ratio, as mentioned in Figure 7. Although this study considers two Venturi nozzle diameter ratios as variables, it can be observed that the influence of internal injector fuel spray holes becomes a determining factor in the spray pattern as the Venturi nozzle diameter ratio increases. In the case of $R_e/R_i = 1.0$, to understand the effect of the geometry of the internal fuel injector hole on the film length, the geometric variables of the fuel injection hole were expressed in terms of velocity and distance with key dimensionless numbers.

$$\left(\frac{F_l}{\dot{m}_a/\dot{m}_l}\right) = \alpha d_0 \left(\frac{\rho_g {V_g}^2}{\rho_l {V_l}^2}\right)^{\beta}, \quad (1)$$

According to other studies investigating breakup length in various injector configurations, the film length indicates a significant correlation with the Reynolds number and Weber number of the oxidizer or fuel, as well as the momentum ratio between the oxidizer and fuel [28–31]. Equation (1) represents the relationship between the momentum flux ratio and the term F_l, divided by the mass flow ratio. This relationship is illustrated in Figure 10. Film lengths are presented depending on the internal fuel injection type, oxidizer pressure and, fuel mass flow rate for all experimental conditions. The determination coefficients for all equations are sequentially 0.65, 0.78, 0.93, and 0.91 from type A to type D. Since Equation (1) does not include variables related to the internal fuel injection characteristics, it follows different curves depending on the injector type. Therefore, to enhance the accuracy of predicting the liquid film size, it is necessary to incorporate additional factors containing these variables into the equation. Therefore, geometric variables related to the location and shape of fuel injection were introduced, and the added variables are displayed in Figure 11.

The position of the fuel injection hole is represented by the distance from the exit of the Venturi nozzle, L_g. In the case of type A, where the angle of the fuel injection location is different, an additional variable, L_l, representing the distance from the fuel injection hole to the wall, was introduced to account for this. L_g and L_l can also be expressed as the horizontal distances traveled by oxidizer and the vertical distances traveled by fuel, respectively. When describing the internal oxidizer velocity (V_g) and fuel velocity (V_l) within the injector, their relationship with length can be expressed in terms of time. The study uses geometric variables within the injector as temporal terms and shares similarities with the research conducted by Choi et al. [32]. By incorporating these terms, the relationship between film length and other terms is expressed as Equation (2). Table 2 illustrates L_g and L_l for each fuel injection column.

$$\left(\frac{F_l}{\dot{m}_a/\dot{m}_l}\right) = \alpha d_0 \left(\frac{\rho_g {V_g}^2}{\rho_l {V_l}^2}\right)^{\beta} \left(\frac{\left(\frac{L_l}{V_l}\right)}{\left(\frac{L_g}{V_g}\right)}\right)^{\gamma}, \quad (2)$$

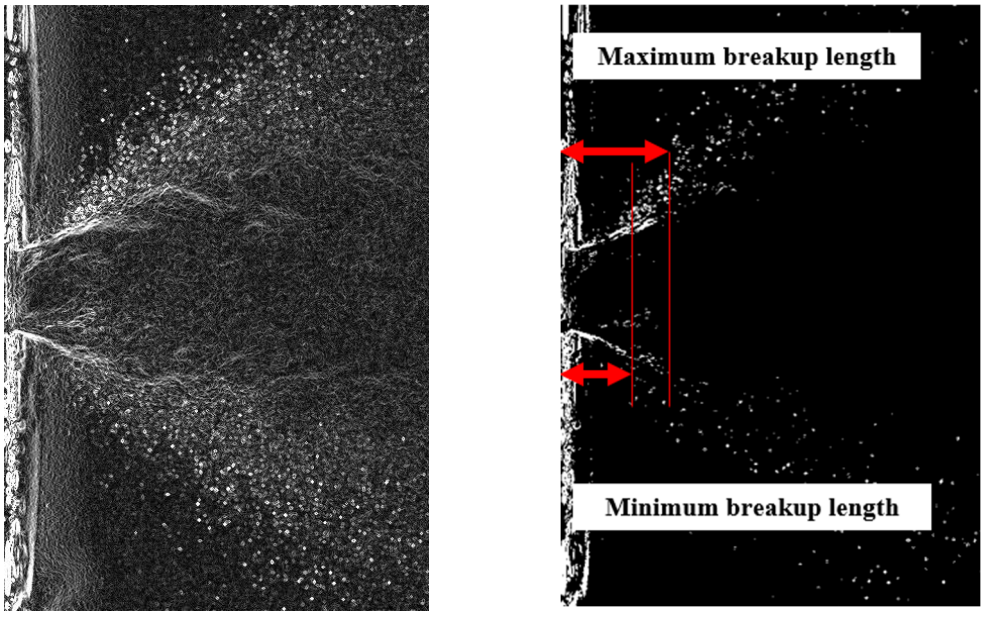

(**a**) (**b**)

Figure 8. Method of measuring the liquid film length: (**a**) density gradient images of Venturi nozzle; (**b**) threshold image of (**a**) and measuring the average length of the liquid film.

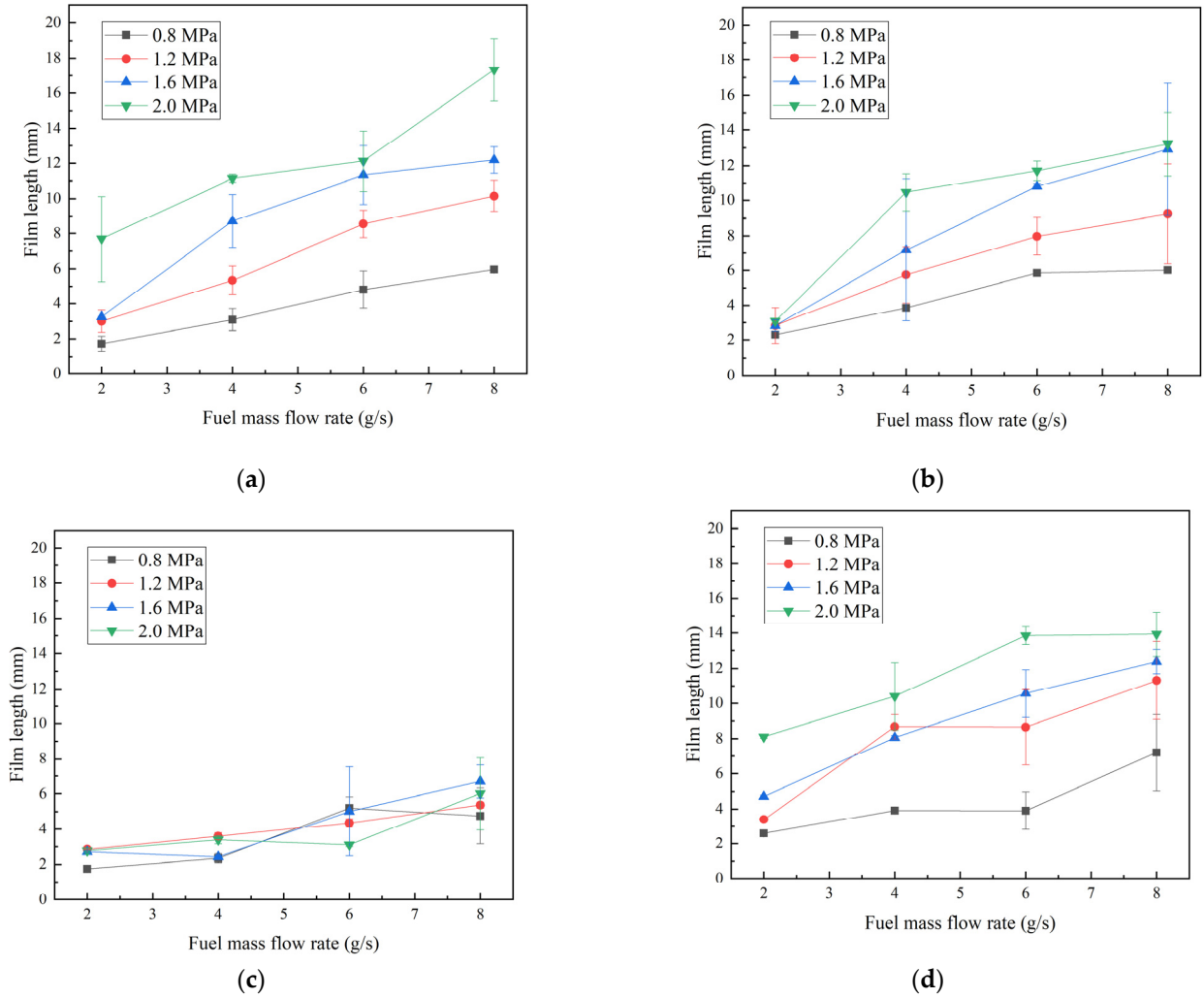

Figure 9. Film length according to the fuel hole type: (**a**) type A; (**b**) type B; (**c**) type C; (**d**) type D.

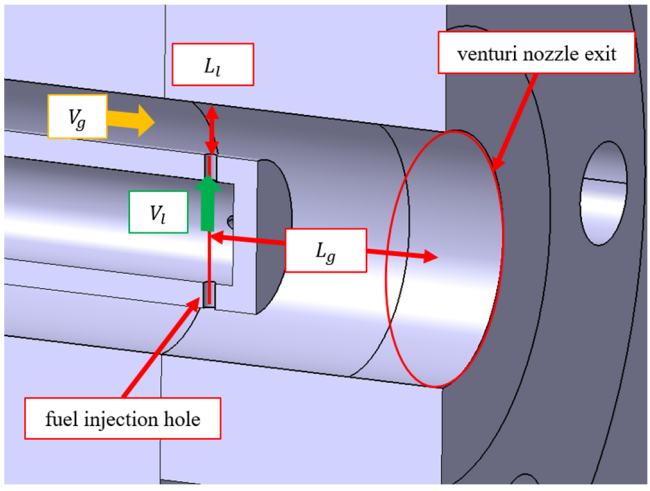

Figure 10. Schematic illustration of the injector describing the velocity and length variables.

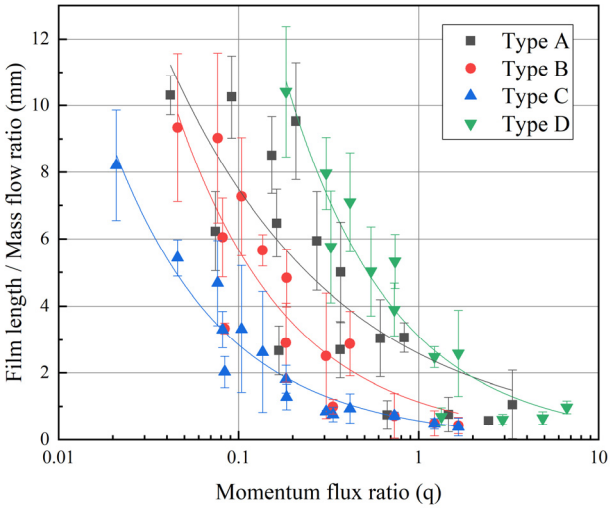

Figure 11. Momentum flux ratio vs. $F_l/\left(\dot{m}_a/\dot{m}_l\right)$ by fuel injection types.

Table 2. L_g and L_l of fuel injection hole type.

Fuel Injection Type	L_g	L_l
Type A	6 mm	3 mm
Type B	6 mm	2 mm
Type C	14 mm	2 mm
Type D	6 mm	2 mm

Equation (2) is obtained by multiplying Equation (1) by length and velocity terms. The relationship depicted in Equation (2) between the momentum flux ratio and the remaining terms can be illustrated, as shown in Figure 12. The y-axis represents all terms except the momentum flux ratio, expressed as the adjusted film length. In other words, incorporating geometric terms in Equation (1) to formulate Equation (2) demonstrates a strong correlation between film length and momentum flux ratio across all the shapes of the fuel injection holes. Therefore, the film length can be predicted based on the geometric shapes of the fuel injection column.

$$\frac{F_l}{d_0} = 2.10 \times 10^{-1} \left(\frac{\rho_g {V_g}^2}{\rho_l {V_l}^2}\right)^{-1.58} \left(\frac{\dot{m}_a}{\dot{m}_l}\right)^{1.00} \left(\frac{\left(\frac{L_l}{V_l}\right)}{\left(\frac{L_g}{V_g}\right)}\right)^{1.60}, \quad (3)$$

Equation (3) represents a re-expression of Equation (2), incorporating the film length and the fuel injection hole diameter, d_0. The dimensions of Equation (2) are standardized by expressing the terms containing F_l as a ratio to d_0, and all the coefficients are explicitly presented.

In this study, when analyzing spray characteristics using spray images, the predominant geometric variable determining the overall spray characteristics is the shape of the Venturi nozzle exit. The number and location of fuel injection holes inside the injector become meaningful variables when the exit area of the Venturi nozzle is sufficiently large.

When the Venturi nozzle throat narrows, resulting in a relatively reduced exit area, the spray mechanism becomes similar to an air-assist atomizer due to increased velocity. Conversely, increasing the exit area of the Venturi nozzle throat results in similar characteristics to an air-blast atomizer. At this point, it is noteworthy that, primarily, the liquid sheet is formed at the exit. Subsequently, it undergoes secondary disintegration into droplets. The size distribution of these droplets is influenced by the internal fuel injector hole configuration. The closer the fuel injector hole is to the Venturi nozzle exit, and the greater

the number of fuel injector holes, the smaller the size and density of the disintegrated droplets become.

In theory, to induce detonation effectively using liquid fuel, a good mixture ratio of fuel–oxidizer is important, requiring uniform atomization of the fuel into small droplets. Visible droplet sizes play a role in decreasing the detonability. Therefore, the possibility of detonation, as indicated by spray characteristics, could depend on the specific design of the detonation device in practical applications.

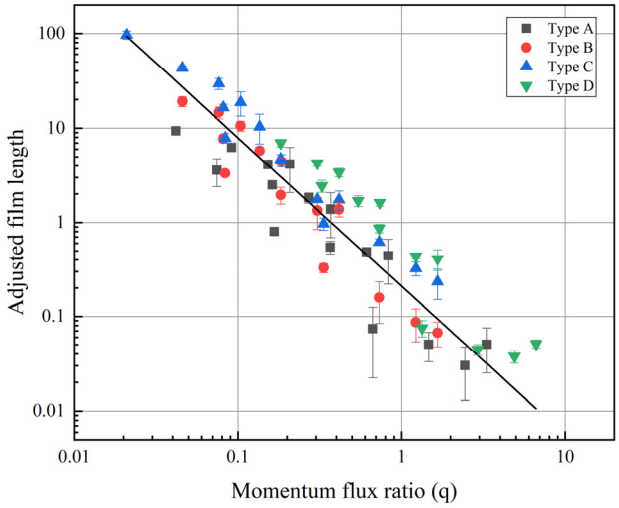

Figure 12. Momentum flux ratio vs. adjusted film length by fuel injection types.

3.2. Droplet Size Distribution

The spray characteristics, based on the shapes of the Venturi nozzle and the injector, were observed using image capture. To achieve a more precise quantitative analysis of droplet distribution, droplet diameter measurements were conducted (shown in Figure 4). The relationship between the measured SMD and the momentum flux ratio is depicted in Figure 13. Figure 13a corresponds to the Venturi nozzle with $R_e/R_i = 0.3$, while Figure 13b represents $R_e/R_i = 1.0$. When the Venturi nozzle diameter is small, there appears to be a certain correlation between the SMD, the position of the fuel hole, and the momentum flux ratio. Overall, an increase in the momentum flux ratio tends to result in a decrease in SMD. This trend is consistent with characteristics of air-assist injectors dominated by air and gas velocities and aligns with similar findings by other researchers [24–27]. For example, Equation (4) represents SMD of an air-assist atomizer, based on the study by Elkotb et al. [33]. The Reynolds number, the Weber number, and the mass flow ratio were utilized as the primary dimensionless numbers, with geometry being fixed.

$$SMD = 51 d_0 Re^{-0.39} We^{-0.18} \left(\frac{\dot{m}_l}{\dot{m}_g} \right)^{0.29}. \quad (4)$$

On the other hand, as the Venturi nozzle diameter increases, observing a clear relationship between the momentum flux ratio and SMD becomes challenging, irrespective of the shape of the fuel hole. These results align with the tendencies of air-blast injectors [28–30]. This sort of tendency, like Equation (5), derived from the research by Bolszo et al., represents a prominent empirical formula for air-blast atomizers utilizing crossflow [31].

$$\frac{d_0}{SMD} = 0.267 We^{0.44} q^{0.08} \left(\frac{\rho_l}{\rho_g} \right)^{0.30} \left(\frac{\mu_l}{\mu_g} \right)^{-0.16}. \quad (5)$$

Therefore, the differentiation of atomization mechanisms can be conducted based not only on spray but also using the relationship between SMD and momentum flux ratio.

Additionally, the average size of SMD is smaller at $R_e/R_i = 0.3$ compared to $R_e/R_i = 1.0$. Depending on the type of fuel injection hole, type D deviates from others. This distribution pattern is attributed to the fact that, with type D, a greater number of holes are present when the same fuel flow rate is injected, resulting in relatively lower jet velocities.

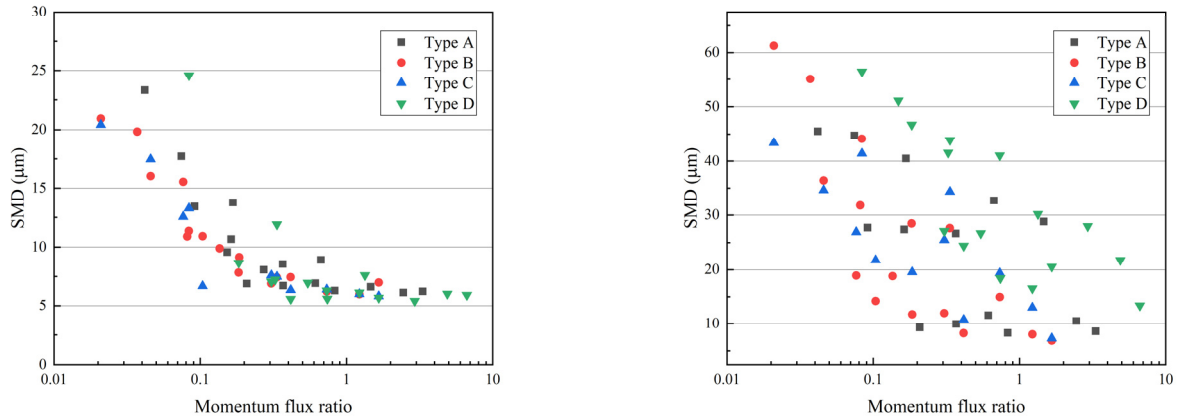

Figure 13. Momentum flux ratio vs. SMD: (**a**) $R_e/R_i = 0.3$; (**b**) $R_e/R_i = 1.0$.

In valveless detonation systems, it is crucial that the droplet size distribution of the liquid fuel is smaller, as this contributes to the faster periodic formation of detonation. Therefore, describing the geometric characteristics of the injector used in this study using key dimensionless numbers allows us to predict the detonability of valveless detonation systems using liquid fuel.

The Venturi nozzle exit diameter determines the oxidizer velocity, which can be expressed in terms of the Reynolds number, a key dimensionless number. Furthermore, as confirmed by using previous spray images and SMD analysis, the spray mechanism applied to the injector varies based on the diameter of the Venturi used in this study. Therefore, the gas velocity term in the Reynolds number is represented by the exit velocity of the Venturi nozzle, $V_{e,g}$, instead of the internal gas velocity, V_g. The Reynolds number using this velocity term is denoted as $Re_{e,g}$.

The fuel velocity depends on the holes inside the injector and the spray direction, expressed using the Weber number. The Weber number is defined with all terms referenced to the fuel, utilizing liquid density, ρ_l, and liquid velocity, V_l, as the bases. Additionally, as shown in Figure 13, the breakup mechanism, dependent on gas velocity and mass, can be explained using momentum flux ratio. To describe the SMD, factors considering the geometric shape of the internal fuel column, including the length ratio, were included. This is similar to explaining the length of the film formed when $R_e/R_i = 1.0$. Equation (6) represents the factors related to the SMD in this experiment, expressed as a product. Numerical analysis using this equation was conducted to predict the SMD.

$$SMD \propto Re_{e,g}^{\alpha} We_l^{\beta} q^{\gamma} \left(\frac{L_g}{L_l}\right)^{\delta}. \quad (6)$$

Equation (7) represents the formula for predicting the overall SMD for all fuel injection types with Venturi nozzle shapes at $R_e/R_i = 0.3$, while Equation (8) does so for $R_e/R_i = 1.0$. The variables included in the equations encompass the gas Reynolds number, the liquid Reynolds number, the momentum flux ratio, the velocity ratio, and the length ratio. The SMD expressions are derived from prior research [32]; additionally, they incorporate a term representing the aspect ratio for predicting film length, accounting for the impact of the locations and the shapes of the fuel injection holes. The influence of $Re_{e,g}$ is notably pronounced across the terms in Equations (7) and (8), underscoring the critical role of Venturi

nozzle velocity in determining spray characteristics. The internal liquid velocity, denoted as We_l in Equation (8) at $R_e/R_i = 1.0$, has a more substantial impact. The momentum flux ratio exhibits a similar influence across all equations. The length ratio, L_g/L_l, exerts limited influence at $R_e/R_i = 0.3$, indicating that the internal fuel spray geometry factor has less impact on spray characteristics when the Venturi nozzle exit diameter is smaller.

$$\frac{SMD}{d_0} = 5.91 \times Re_{e,g}^{-0.55} We_l^{-0.06} q^{-0.31} \left(\frac{L_g}{L_l}\right)^{0.01}, \quad (7)$$

$$\frac{SMD}{d_0} = 3.03 \times Re_{e,g}^{-0.46} We_l^{-0.17} q^{-0.35} \left(\frac{L_g}{L_l}\right)^{0.12}, \quad (8)$$

Figure 14 presents Equations (7) and (8) in (a) and (b), respectively, displaying both the actual SMD and the predicted SMD by using the equations. Each has a coefficient of determination of 0.81 and 0.83. Forming SMD below 5 µm is extremely challenging under room temperature and pressure using conventional atomizer. Therefore, (a) exhibits a narrow SMD distribution, but there is a limit to the distribution since the measured SMD cannot form below a certain diameter. As a result, very small SMDs around 5 µm deviate from the reference. Generally, (b) has a uniform SMD distribution; however, the SMD results for type D deviate from the empirical formula. This phenomenon suggests that additional terms reflecting the internal fuel injection velocity may be necessary. Such correlations can be applied under conditions where the spraying pressure is at ambient temperature and pressure, and the exit velocity is below 150 m/s; these are considered only within the limited range of the experimental conditions used in the present study.

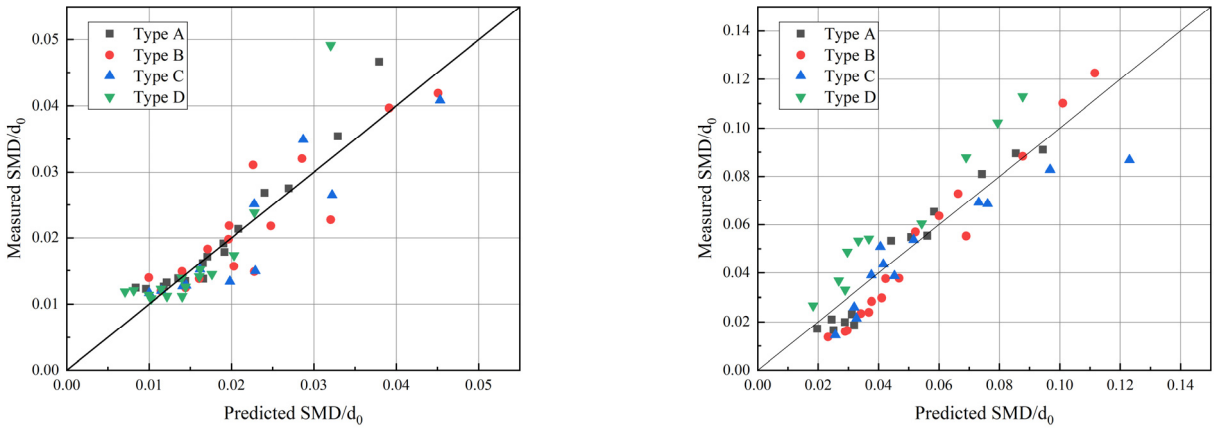

(**a**) (**b**)

Figure 14. Measured SMD vs. predicted SMD: (**a**) $R_e/R_i = 0.3$; (**b**) $R_e/R_i = 1.0$.

4. Discussion and Conclusions

In this study, an injector applicable to a valveless liquid detonation engine was fabricated and experimentally investigated to better understand the effect of spray characteristics on detonation. Building on previous research, an in-liquid fuel injection system was constructed, and the key variables influencing the occurrence of liquid detonation were systematically investigated based on the injector's configuration. High-speed imaging and image analysis were conducted, and SMD measurements were employed to assess injection performance. The conclusions can be summarized in the following key points:

1. The injector used in this study exhibits different spray characteristics based on the diameter ratio of the Venturi nozzle, denoted as R_e/R_i. For $R_e/R_i = 0.3$, the characteristics of an air-assist injector were observed, while for $R_e/R_i = 1.0$, the characteristics of an air-blast injector were evident.

2. Four different fuel injection types were experimented with, varying the injection position, the number of injection holes, and the injection angle. In case of $R_e/R_i = 0.3$, there was almost no significant difference in fuel spray characteristics based on the fuel injection type. However, in the case of $R_e/R_i = 1.0$, different characteristics were observed based on the type of fuel injection hole. Key observations included the formation of liquid films near the Venturi nozzle, and the length of these films varied with the type of fuel injection. The presence or absence of such films could influence the occurrence of detonation. Additionally, factors affecting film length, considering the geometric parameters of the fuel injection hole, were identified, and predicted by empirical correlation.
3. By using SMD measurements, it was confirmed that the fuel spray mechanism varies with R_e/R_i, and a tendency was observed where smaller R_e/R_i values resulted in relatively smaller SMD. To predict SMD, geometric shape factors for predicting film length were introduced, along with length ratio, Reynolds number, and Weber number.
4. Except for type D, the SMD distribution was almost similar among different fuel injection configurations. The Venturi nozzle diameter ratio R_e/R_i had a more significant impact on the overall SMD distribution. This emphasizes that the Venturi nozzle diameter ratio is an important variable that should be carefully considered in designing valveless liquid detonation systems.

In the future, additional experiments are planned, in which we will use the injector employed in this study to investigate the impact of factors such as film length, SMD, and velocity on the actual detonability.

Author Contributions: Conceptualization, M.H.C., Y.O. and S.P.; methodology, M.H.C., Y.O. and S.P.; software, M.H.C., Y.O. and S.P.; validation, M.H.C., Y.O. and S.P.; formal analysis, M.H.C.; investigation, M.H.C., Y.O. and S.P.; resources, M.H.C., Y.O. and S.P.; data curation, M.H.C., Y.O. and S.P.; writing—original draft preparation, M.H.C., Y.O. and S.P.; writing—review and editing, M.H.C., Y.O. and S.P.; visualization, M.H.C., Y.O. and S.P.; supervision, M.H.C., Y.O. and S.P.; project administration, M.H.C., Y.O. and S.P.; funding acquisition, M.H.C., Y.O. and S.P. All authors have read and agreed to the published version of the manuscript.

Funding: This work was partly supported by Korea Institute of Energy Technology Evaluation and Planning (KETEP) grant funded by the Korea government (MOTIE) (20214000000310, Energy Innovation Research Center for Carbon-Neutral High-Efficiency Gas Turbine Combustion Technology) and the National Research Foundation of Korea (NRF) grant funded by the Korea government (MSIT) (NRF-2021K1A3A1A49097854).

Data Availability Statement: The data that support the findings of this study are available from the corresponding author upon reasonable request.

Conflicts of Interest: The authors declare no conflicts of interest.

References

1. Panicker, P.K. The Development and Testing of Pulsed Detonation Engine Ground Demonstrators. Ph.D. Thesis, The University of Texas at Arlington, Arlington, TX, USA, 2008.
2. Schauer, F.; Stutrud, J.; Bradley, R. Detonation Initiation Studies and Performance Results for Pulsed Detonation Engine Applications. In Proceedings of the 39th Aerospace Sciences Meeting and Exhibit, Reno, NV, USA, 8–11 January 2001.
3. Roy, G.D.; Frolov, S.M.; Borisov, A.A.; Netzer, D.W. Pulse Detonation Propulsion: Challenges, Current Status, and Future Perspective. *Prog. Energy Combust. Sci.* **2004**, *30*, 545–672. [CrossRef]
4. Bussing, T.R.A. A Rotary Valved Multiple Pulse Detonation Engine. In Proceedings of the 31st Joint Propulsion Conference and Exhibit, San Diego, CA, USA, 10–12 July 1995; American Institute of Aeronautics and Astronautics Inc., AIAA: Reston, VA, USA, 1995.
5. Hinkey, J.B.; Williams, J.T.; Henderson, S.E.; Bussing, T.R.A. Rotary-Valved, Multiple-Cycle, Pulse Detonation Engine Experimental Demonstration. In Proceedings of the 33rd Joint Propulsion Conference and Exhibit, Seattle, WA, USA, 6–9 July 1997.
6. Matsuoka, K.; Esumi, M.; Ikeguchi, K.B.; Kasahara, J.; Matsuo, A.; Funaki, I. Optical and Thrust Measurement of a Pulse Detonation Combustor with a Coaxial Rotary Valve. *Combust. Flame* **2012**, *159*, 1321–1338. [CrossRef]
7. Lu, W.; Fan, W.; Wang, K.; Zhang, Q.; Chi, Y. Operation of a Liquid-Fueled and Valveless Pulse Detonation Rocket Engine at High Frequency. *Proc. Combust. Inst.* **2017**, *36*, 2657–2664. [CrossRef]

8. Yan, Y.; Fan, W.; Wang, K.; Zhu, X.D.; Mu, Y. Experimental Investigations on Pulse Detonation Rocket Engine with Various Injectors and Nozzles. *Acta Astronaut.* **2011**, *69*, 39–47. [CrossRef]
9. Tucker, K.C.; King, P.I.; Patterson, W.; Oh, A.; Bradley, R.P.; Schauer, F.R. The Use of a Flash Vaporization System with Liquid Hydrocarbon Fuels in a Pulse Detonation Engine. In Proceedings of the 42nd AIAA Aerospace Sciences Meeting and Exhibit 2004, Reno, NV, USA, 5–8 January 2004; p. 868.
10. Brophy, C.; Sinibaldi, D.; Netzer, D.; Johnson, R. Operation of a JP-10/Air Pulse Detonation Engine. In Proceedings of the AIAA 36th Joint Propulsion Conference, Huntsville, AL, USA, 16–19 July 2000.
11. Brophy, C.; Netzer, D.; Forster, D. Detonation Studies of JP-10 with Oxygen and Air for Pulse Detonation Engine Development. In Proceedings of the AIAA 34th Joint Propulsion Conference, Cleveland, OH, USA, 13–15 July 1998.
12. Frolov, S.M.; Basevich, V.Y.; Belyaev, A.A. The Use of Fuel Blends and Distributed Injections for Active Detonability Control in a PDE. In Proceedings of the 17th ICDERS (1999), Heidelberg, Germany, 25–30 July 1999.
13. Fan, W.; Yan, C.; Huang, X.; Zhang, Q.; Zheng, L. Experimental Investigation on Two-Phase Pulse Detonation Engine. *Combust. Flame* **2003**, *133*, 441–450. [CrossRef]
14. Lu, P.L.; Slagg, N.; Fishburn, B.O. Relation of Chemical and Physical Processes in Two Phase Detonation. In Proceedings of the Sixth International Colloquium on Gas Dynamics of Explosion and Reactive Systems, Stockholm, Sweden, 22–26 August 1977.
15. Nicholls, J.A.; Cullen, R.E.; Ragland, K.W. Feasibility Studies of a Rotating Detonation Wave Rocket Motor. *J. Spacecr. Rockets* **1966**, *3*, 893–898. [CrossRef]
16. Bykovskii, F.A.; Zhdan, S.A.; Vedernikov, E.F. Continuous spin detonations. *J. Propuls. Power* **2006**, *22*, 1204–1216. [CrossRef]
17. Lu, F.K.; Braun, E.M. Rotating detonation wave propulsion: Experimental challenges, modeling, and engine concepts. *J. Propuls. Power* **2014**, *30*, 1125–1142. [CrossRef]
18. Xue, S.; Liu, H.; Zhou, L.; Yang, W.; Hu, H.; Yan, Y. Experimental research on rotating detonation with liquid hypergolic propellants. *Chin. J. Aeronaut.* **2018**, *31*, 2199–2205. [CrossRef]
19. Nair, A.P.; Keller, A.R.; Lima, A.; Spearrin, R.M. Deflagration-to-detonation transition in an annular combustor with hypergolic propellants. In Proceedings of the AIAA SCITECH 2022 Forum, San Diego, CA, USA, 3–7 January 2022.
20. Kubicki, S.W.; Anderson, W.; Heister, S.D. Further Experimental Study of a Hypergolically-Ignited Liquid-Liquid Rotating Detonation Rocket Engine. In Proceedings of the AIAA Scitech 2020 Forum, Orlando, FL, USA, 6–10 January 2020.
21. Heister, S.D.; Smallwood, J.; Harroun, A.; Dille, K.; Martinez, A.; Ballintyn, N. Rotating Detonation Combustion for Advanced Liquid Propellant Space Engines. *Aerospace* **2022**, *9*, 581. [CrossRef]
22. Kindracki, J. Experimental Research on Rotating Detonation in Liquid Fuel-Gaseous Air Mixtures. *Aerosp. Sci. Technol.* **2015**, *43*, 445–453. [CrossRef]
23. Lim, D.; Heister, S.D.; Humble, J.; Harroun, A.J. Experimental Investigation of Wall Heat Flux in a Rotating Detonation Rocket Engine. *J. Spacecr. Rockets* **2021**, *58*, 1444–1452. [CrossRef]
24. Lefebvre, A.H.; McDonell, V.G. *Atomization and Sprays*; CRC Press: Boca Raton, FL, USA, 2017.
25. Mlkvik, M.; Stähle, P.; Schuchmann, H.P.; Gaukel, V.; Jedelsky, J.; Jicha, M. Twin-Fluid Atomization of Viscous Liquids: The Effect of Atomizer Construction on Breakup Process, Spray Stability and Droplet Size. *Int. J. Multiph. Flow* **2015**, *77*, 19–31. [CrossRef]
26. Li, Z.; Wu, Y.; Cai, C.; Zhang, H.; Gong, Y.; Takeno, K.; Hashiguchi, K.; Lu, J. Mixing and Atomization Characteristics in an Internal-Mixing Twin-Fluid Atomizer. *Fuel* **2012**, *97*, 306–314. [CrossRef]
27. Rizk, N.K.; Lefebvre, A.H. H. Spray Characteristics of Plain-Jet Airblast Atomizers. *J. Eng. Gas Turbines Power* **1984**, *106*, 634–638. [CrossRef]
28. Warncke, K.; Gepperth, S.; Sauer, B.; Sadiki, A.; Janicka, J.; Koch, R.; Bauer, H.J. Experimental and numerical investigation of the primary breakup of an airblasted liquid sheet. *Int. J. Multiph. Flow* **2017**, *91*, 208–224. [CrossRef]
29. Gepperth, S.; Müller, A.; Koch, R.; Bauer, H.J. Ligament and droplet characteristics in prefilming airblast atomization. In Proceedings of the ICLASS, 12th Triennial International Annual Conference on Liquid Atomization and Spray Systems, Heidelberg, Germany, 2–6 September 2012; pp. 1–8.
30. Kumar, A.; Sahu, S. Influence of nozzle geometry on primary and large-scale instabilities in coaxial injectors. *Chem. Eng. Sci.* **2020**, *221*, 115694. [CrossRef]
31. Bolszo, C.D.; McDonell, V.G.; Gomez, G.A.; Samuelsen, G.S. Injection of water-in-oil emulsion jets into a subsonic crossflow: An experimental study. *At. Sprays* **2014**, *24*, 303–348. [CrossRef]
32. Choi, M.H.; An, J.; Koo, J. Breakup Mechanism of a Jet in the L-Shape Crossflow of a Gas Turbine Combustor. *Energies* **2022**, *15*, 3360. [CrossRef]
33. Elkotb, M.; Mahdy, M.; Montaser, M. Investigation of external-mixing airblast atomizers. In Proceedings of the 2nd International Conference on Liquid Atomization and Sprays, Madison, WI, USA, 20–24 June 1982; pp. 107–115.